Arch. Metall. Mater. **65** (2020), 1, 5-14

DOI: 10.24425/amm.2019.131091

R. SHASHANKA[1*], ORHAN UZUN[2], D. CHAIRA[3]

SYNTHESIS OF NANO-STRUCTURED DUPLEX AND FERRITIC STAINLESS STEEL POWDERS BY DRY MILLING AND ITS COMPARISON WITH WET MILLING

In the present paper, elemental Fe, Cr and Ni powders were used to fabricate nano-structured duplex and ferritic stainless steel powders by using high energy planetary ball milling. We have studied the effect of milling atmosphere like wet (toluene) and dry (argon) milling of elemental Fe-18Cr-13Ni (duplex) and Fe-17Cr-1Ni (ferritic) powders for 10 h in a dual drive planetary mill. Stearic acid of 1wt. % was added during milling to avoid agglomeration. The dry and wet milled duplex and ferritic stainless steel powders were characterized by XRD, SEM and particle size analysis techniques. We have found that both the milling atmospheres have great influence in controlling the final particle morphology, size and phase evolution during milling. It was reported that dry milling is more effective in reducing particle size than the wet milling. The Nelson-Riley method of extrapolation was used to calculate the precise lattice parameter and Williamson-Hall method was used to calculate the crystallite size and lattice strain of both the stainless steel milled in argon atmosphere. Dry milled duplex and ferritic stainless steel were then consolidated by conventional sintering method at 1100, 1200 and 1300°C temperatures under argon atmosphere for 1 hour.

Keywords: Powder metallurgy; dry and wet milling; planetary milling; stainless steel; sintering

1. Introduction

Due to the wide range of properties and applications; stainless steel has become one of the very important engineering materials. Duplex stainless steel and ferritic stainless steel are the two grades of stainless steel used in almost everywhere. Duplex stainless steel has both the properties of austenite and ferritic stainless steel; this is due to the amalgamation of almost equal proportions of austenite and ferrite. The differences in the proportions can alter the properties; and it mainly depends upon the composition, method of preparation and experimental conditions. The amalgamated effect of duplex stainless steel impart an excellent corrosion resistance, high energy absorption, high strength, low thermal expansion, good weldability, good high-temperature tensile and creep strength [1]. Due to its extensive properties; one can employ the duplex stainless steel in marine, chemical, petrochemical, nuclear power, oil, paper and pulp industries [2-4]. Whereas, ferritic stainless steel can be used in water treatment plants, refrigeration cabinets, chemical and food processing, cold water tanks, street furniture, electrical cabinets, storing knives, sticking memos on the fridge and other metallic implements [5]. The wide range applications of ferritic stainless steel are mainly due to the excellent properties like less stress corrosion, high thermal conductivity, excellent high temperature oxidation resistance, creep resistance, low thermal expansion, high yield strength and magnetic properties [6,7]. Generally, ferritic stainless steel is having body centered cubic lattice structure and contains less amount of expensive Ni.

Most of the materials show splendid properties and broad range of applications with decrease in the size to nano level [8]. Therefore, scientists are trying to reduce the structure of stainless steels to nano to improve the properties and extend their applications [9]. There are many methods available to reduce the crystallite size of stainless steels, but mechanical alloying is one of the most widely accepted plastic deformation method used to refine the structures of materials to nano range [10-12]. The advantage of mechanical alloying lies in the production of extremely fine materials in large amount within a very shorter time intervals and henceforth, reduces the possibility of oxidation of materials [13].

Mechanical alloying process can be operated under dry or wet condition. In dry milling process, typical parameters like milling equipment, milling energy, milling time, ball to powder

[1] BARTIN UNIVERSITY, DEPARTMENT OF METALLURGICAL AND MATERIALS ENGINEERING, BARTIN-74100, TURKEY
[2] RECTORATE OF BARTIN UNIVERSITY, BARTIN-74100, TURKEY
[3] NATIONAL INSTITUTE OF TECHNOLOGY, DEPARTMENT OF METALLURGICAL AND MATERIALS ENGINEERING, ROURKELA-769008, INDIA

* Corresponding author: shashankaic@gmail.com

weight ratio, particle nature (ductile/brittle) and feed size can affect the properties of powder particles. Whereas, in wet milling the properties such as viscosity, solid concentrate and pH can alter the properties of powder suspension [14]. Dry milling share the same design as that of wet milling, but in dry milling argon gas was used whereas in wet milling toluene was used. Due to the less hindrance of gas for the movement of balls inside the milling jars; dry milling takes more advantage of centrifugal force and the coriolis effect to grind materials to a very fine or even nano size [15]. On the other hand; in wet milling the movement of balls inside the milling jars are hindered by the toluene and leads to less effective size reduction of materials.

Therefore, in the present paper we have prepared nano-structured duplex and ferritic stainless steel powders from elemental compositions using specially designed dual drive planetary mill (DDPM) by dry milling method and studied the effect of milling medium (dry and wet milling) on the microstructure of both the stainless steels. The design of the mill and fabrication of duplex and ferritic stainless steels by wet milling was reported by the authors elsewhere [16]. In another set of experiment, we consolidated the 10 h dry milled nano-structured duplex and ferritic stainless steel powders. Consolidation at different sintering temperature was performed to study its effect on hardness, density, wear resistance and possible phase transformation. Many researchers including the author had published papers on consolidation of stainless steel after wet milling, but, very limited publications are reported on consolidation of stainless steel after dry milling.

Ismail et al. synthesized $Ni_{0.5}Zn_{0.5}Fe_2O_4$ alloy at different ball to powder weight ratio (BPR) (4:1, 6:1, 8:1, 10:1, 12:1, 14:1, 16:1, 18:1 and 20:1) by using SPEX 8000D shaker mill and studied the microstructure of the alloy. They reported that, up to 16:1 BPR the crystallite size decreases and then start increasing with increase in BPR due to cold welding. Similarly, strain goes on increasing up to 16:1 BPR and after that it will start to decrease [17]. Shashanka et al. prepared nano-structured duplex and ferritic stainless steel by wet milling using high energy dual drive planetary ball mill. They reported that, as the milling time increases the crystallite size decreases, strain increases and particle size decreases [16,18-20]. They consolidated the prepared stainless steel powders using hydraulic pressing at 700 MPa and sintered at 1000, 1200 and 1400°C respectively and studied the effect of sintering temperature on the microstructure, hardness, density and wear resistant properties [21-24]. Pandya et al. studied the densification of austenitic stainless steel at different sintering temperatures 1200, 1300, 1400°C respectively to study their effect on the microstructure and mechanical properties of austenitic stainless steel. They correlated processing parameters, microstructure, and properties and concluded that increase in sintering temperature increases the density of austenitic stainless steel [25]. Vijayalakshmi et al. reported the microstructural variation and mechanical properties of duplex stainless steel sintered at 1100, 1200, 1300 and 1350°C respectively. They concluded that the surface hardness mainly depends upon the phases present in the materials [26]. Shashanka et al. studied the effect of BPR, mill speed, mill time, process controlling agents in their previous publication. They concluded that, all these milling parameters play an important role on powder morphology, size and phase transformation [5].

Therefore, we reported the effect of milling atmosphere (dry milling and wet milling) in the present paper. We have made a successful attempt to prepare nano-structured duplex and ferritic stainless steel powders by an efficient dry milling method.

2. Experimental

2.1. Preparation of nano-structured duplex and ferritic stainless steel powder by dry milling

Elemental powder mixture of Fe (99.5% pure), Cr (99.8% pure) and Ni (99.5% pure) were used as starting materials for dry milling. The average particle size of iron powder is <10 μm, nickel is <45 μm and chromium is <50 μm respectively. The elemental compositions of duplex (Fe-18Cr-13Ni) and ferritic stainless steels (Fe-17Cr-1Ni) were selected from Schaeffler diagram [27]. Dry milling of the above composition was carried out in a specially designed dual drive planetary mill (DDPM) for 10 h under argon atmosphere to prevent oxidation. Critical speed of the mill and ball to powder weight ratio were maintained at 64% and 6:1 respectively. Stainless steel jars of volume one litre (1 L) and 8 mm diameter high chrome steel balls of 1 kg were used as grinding vessel and grinding media respectively. The jar was filled with argon gas to maintain inert atmosphere to reduce the oxidation of stainless steel. The same experimental setup and conditions were used for wet milling also, but instead of argon gas; toluene was used. Milled powders were characterized by X-ray diffraction (XRD) in a Philips PANalytical diffractometer using filtered Cu Kα-radiation (λ = 0.1542 nm) at different time intervals of milling. Crystal size and lattice strain of the milled powders were calculated using Williamson Hall method. Nelson-Riley (N-R) method of extrapolation was used to calculate lattice parameter. Powder morphology was studied by scanning electron microscopy (SEM) using JEOL JSM-6480LV and particle size was measured by Malvern Mastersizer.

2.2. Consolidation of nano-structured duplex and ferritic stainless steel by conventional sintering method

Nano-structured duplex and ferritic stainless steel powder samples after 10 h of dry milling in DDPM were compacted using hydraulic pressing machine under a pressure of 700 MPa using polyvinyl alcohol as a binder. The compacted pellets were sintered respectively at 1100, 1200 and 1300°C in an argon atmosphere with a holding time of 1 h each and all the sintered stainless steel samples were furnace cooled. The sintered pellets were then polished carefully and their density and hardness were measured by Archimedes [28] and Vickers microhardness methods [29] respectively. Vickers microhardness studies were carried out using LECO-LM248AT fitted with a Vickers pyramidal diamond intender. The microhardness studies were

carried out at three different loads 98, 245 and 490 mN to study the effect of load on hardness with a dwell time of 10 seconds for all the trials and samples. The 5 trials of indentation of each sample were made with different loads and the average values of the diagonal lengths of indentation marks were measured. Microstructural study of conventionally sintered stainless steel samples were carried out by using Carl Zeiss optical microscope.

3. Results and discussion

3.1. Synthesis of nano-structured stainless steel powder

3.1.1. X-ray diffraction study

Figure 1(a) and 1(b) depict the XRD spectra of duplex and ferritic stainless steel powders respectively milled in argon atmosphere at different milling time. As milling continues, the sharp crystalline peaks of elemental Fe, Cr and Ni begin to broaden continuously with milling and eventually move into the lattice of Fe. The dry milled duplex and ferritic stainless steel samples show very broad peaks with decreased intensity when compared with wet milled stainless steel samples as shown in the Figure 1(c) and 1(d) respectively. This is due to the effective rate collision of balls with powder particles during dry milling when compared with wet milling. The impact energy generated during dry milling is more as the balls can freely move inside the jars as there is no liquid media to hinder the ball and particle movement. This increases the effective collision of ball-jar-powder; hence dry milling results in decreased crystallite size and increased strain when compared with wet milled samples. We can also observe a shift of α-Fe (110) peak towards lower angle side after milling to 10 h as shown in the figure 1(c). This displacement of (110) peak is due to the formation of austenite phase along with ferrite phase and confirms the presence of dual phase duplex stainless steel.

3.1.1.1. Lattice parameter calculation

Nelson-Riley (N-R) extrapolation method was used to calculate the true lattice parameters by using the below relation [31],

$$\frac{\cos^2\theta}{\sin\theta}+\frac{\cos^2\theta}{\theta} \qquad (1)$$

During lattice parameter calculation, three strong XRD peaks of individual duplex and ferritic stainless steel powders

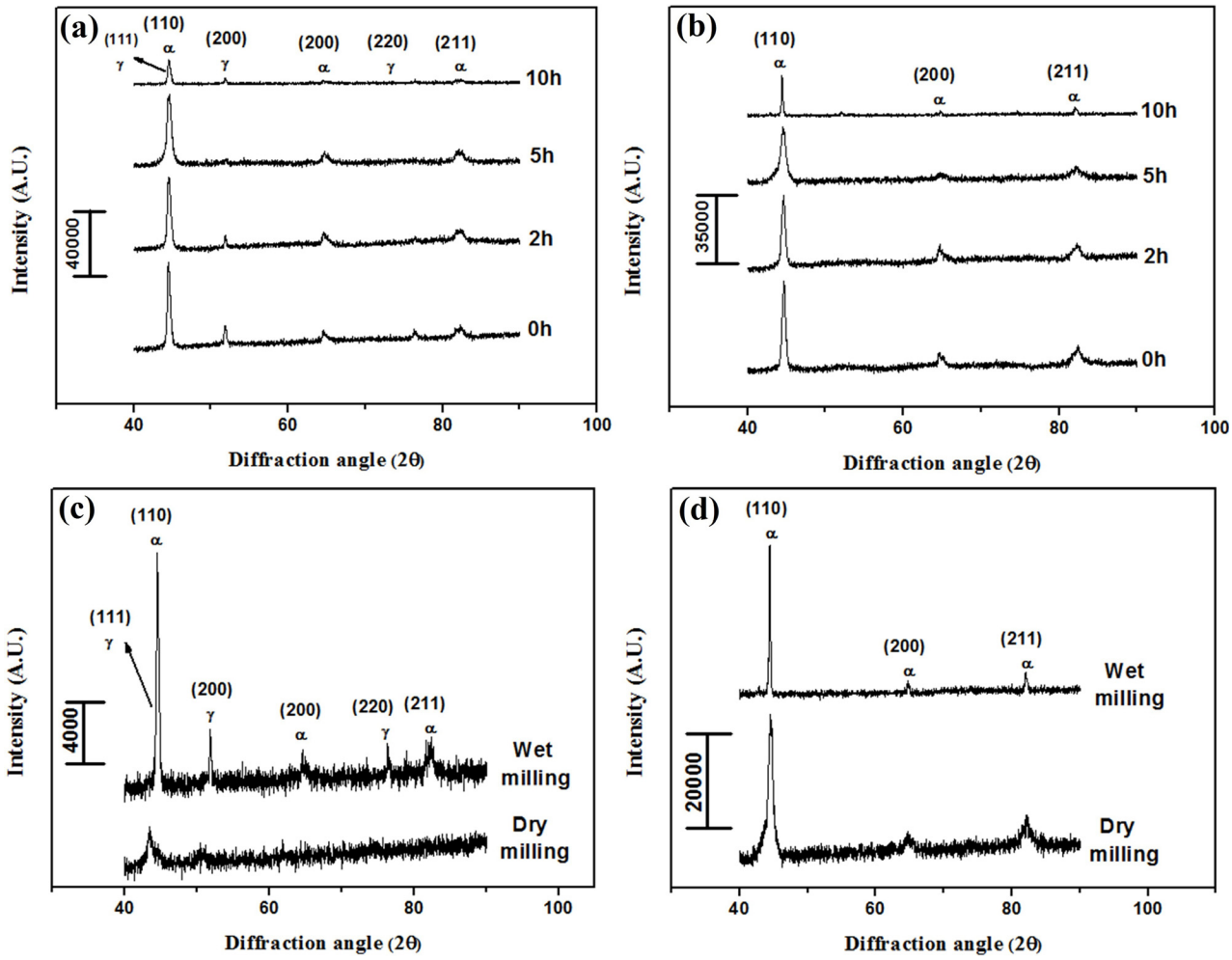

Fig. 1. XRD spectra of 0 to 10 h dry milled (a) Duplex stainless steel (b) Ferritic stainless in argon atmosphere; Comparison of 10 h milled (c) Duplex stainless steel (d) Ferritic stainless steel by wet and dry milling

were taken and N-R functions were calculated for each peak. Then lattice parameter for each peak was calculated and the values were fitted in a straight line and extrapolated the straight line to y-axis. The point of intersection on y-axis gives the true lattice parameter value [16]. Figure 2(a) and 2(b) show true lattice parameter of duplex and ferritic stainless steel samples milled in argon and toluene atmospheres respectively. In wet milling there is a hindrance of balls and powder collisions by toluene but this type of hindrance is absent in dry milling. This increases the impact energy of collision during dry milling. Hence, the amount of defects formed during dry milling is more than the defects formed during wet milling. Therefore, lattice parameter value of dry milled duplex and ferritic stainless steel is more compared with wet milled samples. True lattice parameter value of austenite present in duplex and pure ferritic stainless steel powder milled at argon atmosphere is 3.471 Å and 2.875 Å respectively and that of toluene atmosphere is 3.43 Å and 2.870 Å respectively.

3.1.1.2. Crystallite size and lattice strain calculation

Generally, diffraction peak broadening will take place due to the instrumental errors, decrease in particle size and increase in lattice strain. The peak broadening resulting from the instrumental errors can be minimized by using Williamson-Hall equation [5]. Williamson and Hall proposed a method for de-convoluting size and strain broadening by looking at the peak width as a function of 2θ. Using XRD data, we determined crystallite size and lattice strain using Williamson-Hall equation [21,31] as follows:

$$\beta \cos\theta = \frac{0.94\lambda}{D} + 4\eta \sin\theta \qquad (2)$$

Where, β is full width half maxima (FWHM), D is crystallite size and h is lattice strain.

Crystallite size and lattice strain can be calculated by plotting sinθ on the x-axis and β cosθ on the y-axis (β in radians). From the linear fit, crystallite size and lattice strain are extracted from intercept and slope respectively. The three strong peaks of both duplex and ferritic stainless steel were used for the determination of crystallite size and lattice strain.

Figure 3(a) and 3(b) depicts the crystallite size and lattice strain of duplex and ferritic stainless steel powder milled in argon and toluene atmospheres respectively. From the graph it is confirmed that, the crystallite size decreases with increase in milling time and it attains a saturation level after 10 h, where further refinement of crystallite size is very difficult. However, lattice strain goes on increasing with increase in milling time as shown in Figure 3(a) and Figure 3(b). From the figure it is also clear that crystallite size of dry milled duplex and ferritic stainless steel is less compared to wet milled stainless steel samples. Similarly, lattice strain of both the stainless steel is more during dry milling than wet milling. This is because; dry milling involves high impact energy, results in more dislocations and hence high lattice strain. The crystallite size and lattice strain of duplex stainless steel milled in argon atmosphere is 6 nm and 21.8×10^{-3} and in toluene atmosphere is 7nm and 9.98×10^{-3} respectively. Similarly, dry milled ferritic stainless steel has crystallite size of 8nm and lattice stain of 30×10^{-3} and wet milled ferritic stainless steel has crystallite size of 10nm and lattice strain of 9.47×10^{-3} respectively. Meng et al. reported that as the grain size of pure iron reaches below 14 nm then austenite phase become more stable [32]. The crystallite sizes of prepared duplex and ferritic stainless steel powders are well below 14 nm and therefore phase transformation takes from α-Fe to γ-Fe during milling (Phase transformation from α-Fe to γ-Fe is also confirmed by XRD studies).

3.1.2. Scanning electron microscopy (SEM)

Figure 4(a-d) and 4(f-i) represent the SEM micrographs of 0, 2, 5 and 10 h milled duplex and ferritic stainless steel powders under argon atmosphere. Figure 4(e) and 4(j) show the micrographs of duplex and ferritic stainless steel milled for 10 h in toluene atmosphere (Wet milling). From SEM figures it is evident that stainless steel milled in argon (dry milling) atmosphere shows lesser particle size compared to stainless

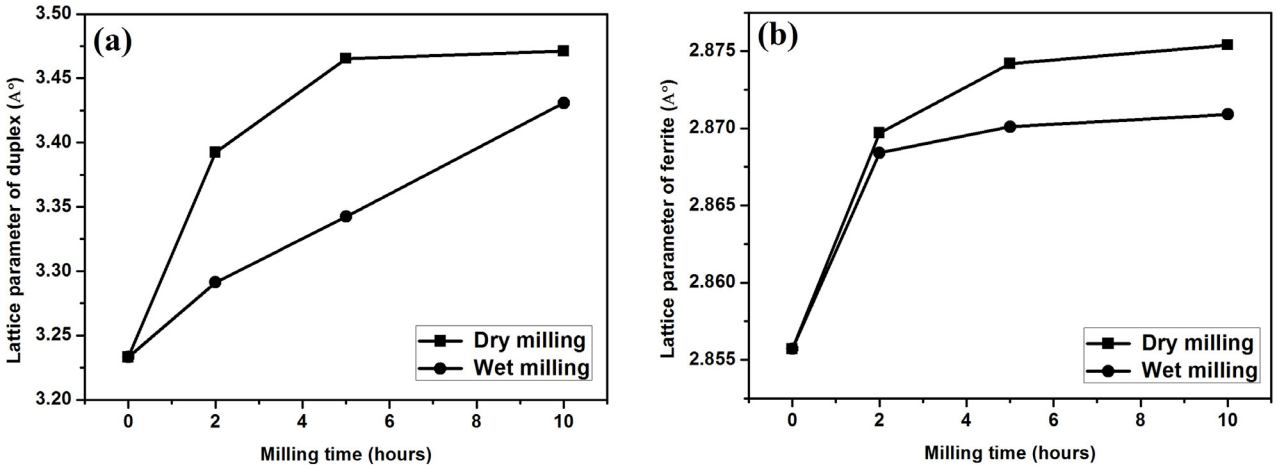

Fig. 2. Graphical representation showing the effect of milling atmosphere on the lattice parameter (calculated from Nelson-Riley extrapolation method) of (a) Duplex stainless steel (b) Ferritic stainless steel during dry milling (argon) and wet milling (toluene) respectively

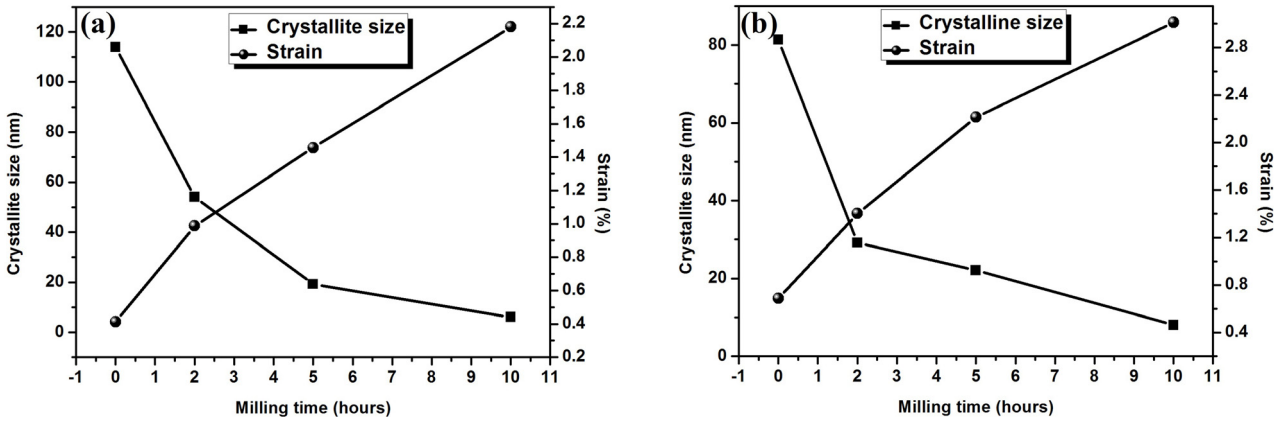

Fig. 3. Graphical representation showing the variation of crystallite size and strain (Calculated from Williamson-Hall method) with milling time of (a) Duplex stainless steel (b) Ferritic stainless steel milled at argon atmosphere

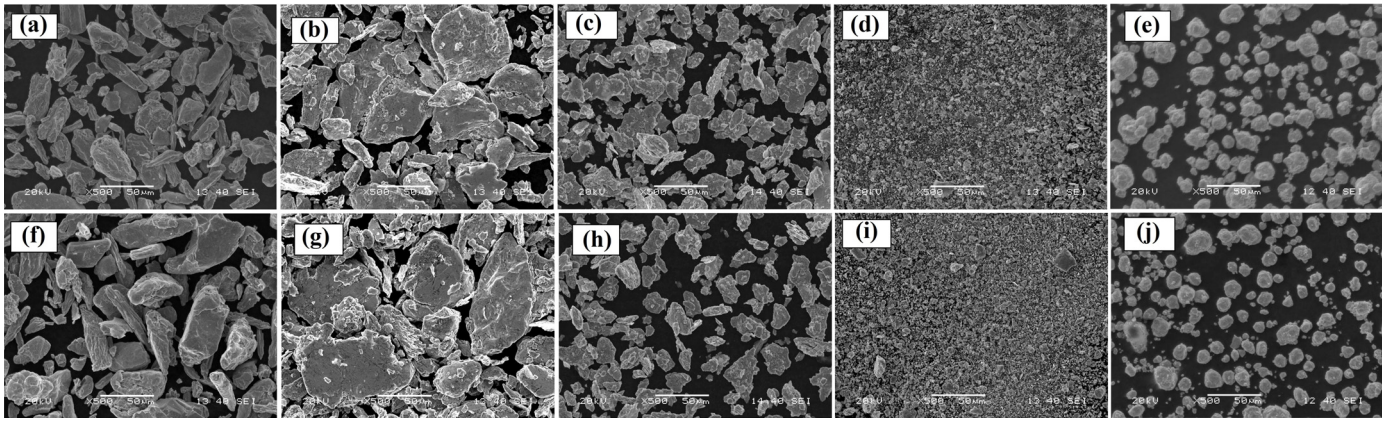

Fig. 4. SEM images of duplex stainless steel powders milled for (a) 0 h (b) 2 h (c) 5 h (d) 10 h at argon atmosphere, and (e) 10 h at toluene atmosphere. SEM images of ferritic stainless steel powder milled for (f) 0 h (g) 2 h (h) 5 h (i) 10 h at argon atmosphere, and (j) 10 h at toluene atmosphere

steel powders milled in toluene (wet milling) atmosphere. In wet milling, balls-jar-powder collisions had been hindered by toluene due to its viscous nature when compared to argon gas. As a result, milling in argon atmosphere enhances the free mobility of balls and impact energy of collision. This in turn increases the rapid cold welding, work hardening and fine fragmentation of stainless steel particles readily at short time.

3.1.3. Particle size analysis

The particle size distribution of 0 to 10 h milled duplex and ferritic stainless steel powder samples in argon atmosphere and 10 h milled stainless steel samples in toluene atmosphere are depicted in figure 5(a) and 5(b) respectively. The dry milled duplex and ferritic stainless steel powders show extremely lesser

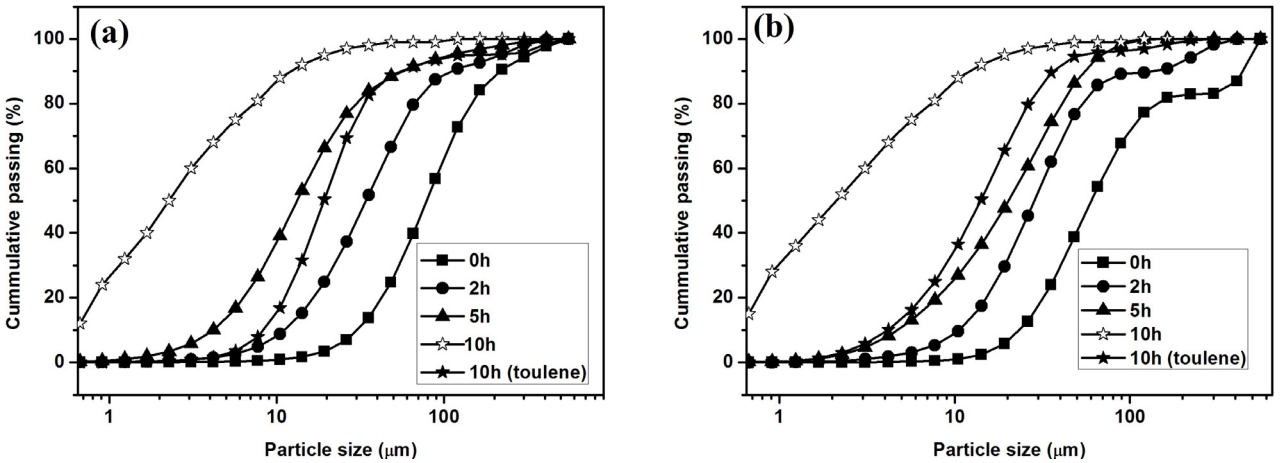

Fig. 5. Particle size analysis of 0 to 10 h milled (a) Duplex stainless steel (b) Ferritic stainless steel during dry milling and 10 h wet milled samples

particle size than wet milled powder samples as shown in figure. The median particle size of 10 h dry milled duplex and ferritic stainless steel samples are found to be 3 and 2 μm respectively, whereas the median size is 20 and 16 μm in case of 10 h wet milled duplex and ferritic stainless steel samples. Wet milling was conducted under toluene and hence viscosity of suspension reduces the reduction rate as damping action takes place between grinding media and steel powder. On the other hand, no such suspension was formed during dry milling. Hence, faster grinding takes place in dry grinding than wet grinding.

Our results are comparable with the results obtained by different researchers. Some of the researchers investigated the microstructural evolution, particle shape and size of duplex and ferritic stainless steel powders by optimizing the milling parameters and their results are tabulated in Table 1.

3.2. Consolidation of stainless steel powders

3.2.1. X-ray diffraction study

The XRD spectra of dry milled duplex and ferritic stainless steel samples sintered at 1100, 1200 and 1300°C are shown in figure 6(a) and 6(b) respectively. The XRD spectra of conventionally sintered duplex and ferritic stainless steels show sharp and crystalline diffraction peaks of the ferrite and the austenite phases. From the XRD spectra, we can observe the enhanced crystallinity of diffraction peaks with increase in sintering temperature from 1100 to 1300°C. During dry milling of duplex and ferritic stainless steel, they had undergone many transformations like introduction of structural defects, amorphization, reduction in crystallite size, increase in lattice strain and volume fraction of grain boundaries [21]. This results in increased number of defect storage sites, shortens diffusion paths and attains non-equilibrium state [39]. During sintering, both the stainless steel powder particles diffuse through necking and rearrange themselves in a regular manner and in turn increases the crystallinity of stainless steel, rate of diffusion, grain growth and the atomic periodicity. Duplex stainless steel shows phase transformation from α-Fe to γ-Fe during sintering and results in more dominant austenite phase at higher temperature due to the high temperature stability of austenite phase [40]. The phase transformation may be due to the diffusion of Cr and Ni atoms into the smaller interstitial sites of ferrite crystallites and which forms mismatch strains and thus initiate phase transformation [16]. The refinement of ferrite crystallite to nano-level can also initiate phase transformation [21]. Both the XRD spectra show no sign of sigma phases, carbides or nitride precipitations of secondary phases.

TABLE 1

A comparison on fabrication of duplex and ferritic stainless steel powders by mechanical alloying method among different investigators and present research

References	Type of stainless steel	Type of mill	Milling time (hours)	Milling media	Crystallite size (nm)	Particle size (μm)	Particle morphology
[33]	Duplex	Planetary ball mill	60	Jar volume: 120 ml, 6:1 BPR, Argon atmosphere,	15	—	—
[34]	Austenite	Retsch PM100	100	Jar volume: 500 ml, 25:1 BPR, 300 rpm mill speed, Nitrogen atmosphere,	<10	200	Irregular shape with agglomeration
[35]	Yittria dispersed austenite	High energy planetary mill	50	Different ball sizes 20, 10 and 6 mm, 5:1 BPR, 300 rpm mill speed, Nitrogen atmosphere,	13	100	Nearly spherical with different sizes
[36]	Austenite	Retsch PM100	100	Balls with 20 mm diameter, 25:1 BPR, 300 rpm mill speed, Nitrogen atmosphere	7	7	Irregular shape and sizes
[37]	Ferritic stainless steel	Sepahan planetary ball mill	120	Jar volume: 150 ml, Balls with 20 and 12 mm diameter, 20:1 BPR, 500 rpm mill speed, argon atmosphere	10	—	—
[38]	Yittria dispersed ferritic stainless steel	Simoloyer CM20 horizontal ball mill	48	15:1 BPR, 240 rpm mill speed, Ar-H_2 mixture atmosphere	—	60	Spherical shape with a smooth surface
[16]	Duplex stainless steel	High energy planetary mill	10	Jar volume: 1000 ml, 1000 g chrome steel balls, 6:1 BPR, Toluene atmosphere	7	22	Spherical particles with more regularity
[16]	Ferritic stainless steel	High energy planetary mill	10	Jar volume: 1000 ml, 1000 g chrome steel balls, 6:1 BPR, Toluene atmosphere	8	16	Spherical particles with more regularity
[Present paper]	Duplex stainless steel	High energy planetary mill	10	Jar volume: 1000 ml, Balls with 8 mm diameter, 6:1 BPR, critical mill speed is 64%, argon atmosphere	6	3	Nearly spherical with almost same sizes
[Present paper]	Ferritic stainless steel	High energy planetary mill	10	Jar volume: 1000 ml, Balls with 8 mm diameter, 6:1 BPR, critical mill speed is 64%, argon atmosphere	8	2	Nearly spherical with almost same sizes

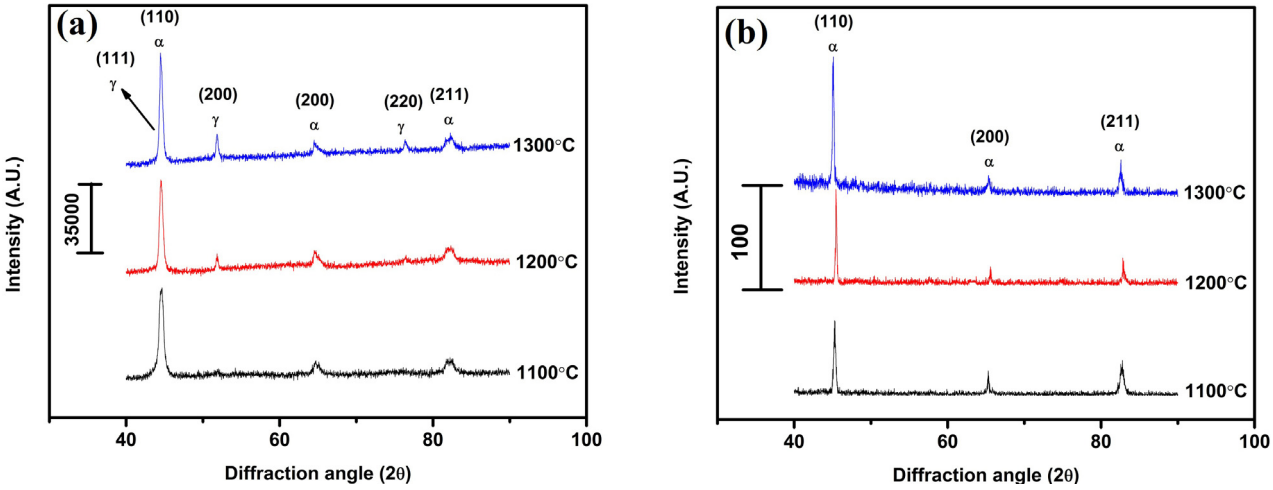

Fig. 6. XRD spectra of (a) duplex and (b) ferritic stainless steel samples sintered at 1100, 1200 and 1300°C respectively in argon atmosphere

3.2.2. Microstructure analysis

Figure 7(a) and 7(b) depicts the optical micrographs of duplex and ferritic stainless steel samples consolidated at 1100, 1200 and 1300°C respectively. From the optical microstructures, we can observe that the porosity ratio decreases with the increase in sintering temperature from 1100 to 1300°C. This is due to rapid rate of mass transfer at higher temperatures through necking and results in fewer pores [23]. The duplex stainless steel sintered at 1300°C contains acicular ferrite as shown in figure 7(a). The acicular ferrite is characterized by needle shaped chaotic grains of ferrite usually formed in the interior of austenite phase by nucleation. This chaotic order acts as obstacles for cleavage, crack propagation and hence increases the strength of stainless steel [22, 41]. Shashanka et al. [22] and Ricks et al. [42] reported that dispersion of oxygen rich non-metallic inclusions results in the formation of acicular ferrites. Moreover, the formation of grain and grain boundaries are also observed in ferritic stainless steel sintered at 1200 and 1300°C as evident in figure 7(b). It is also observed that grain growth takes place as sintering temperature increases.

3.2.3. Density and hardness study

The effect of sintering temperatures (1100, 1200 and 1300°C) on the densities of duplex and ferritic stainless steel

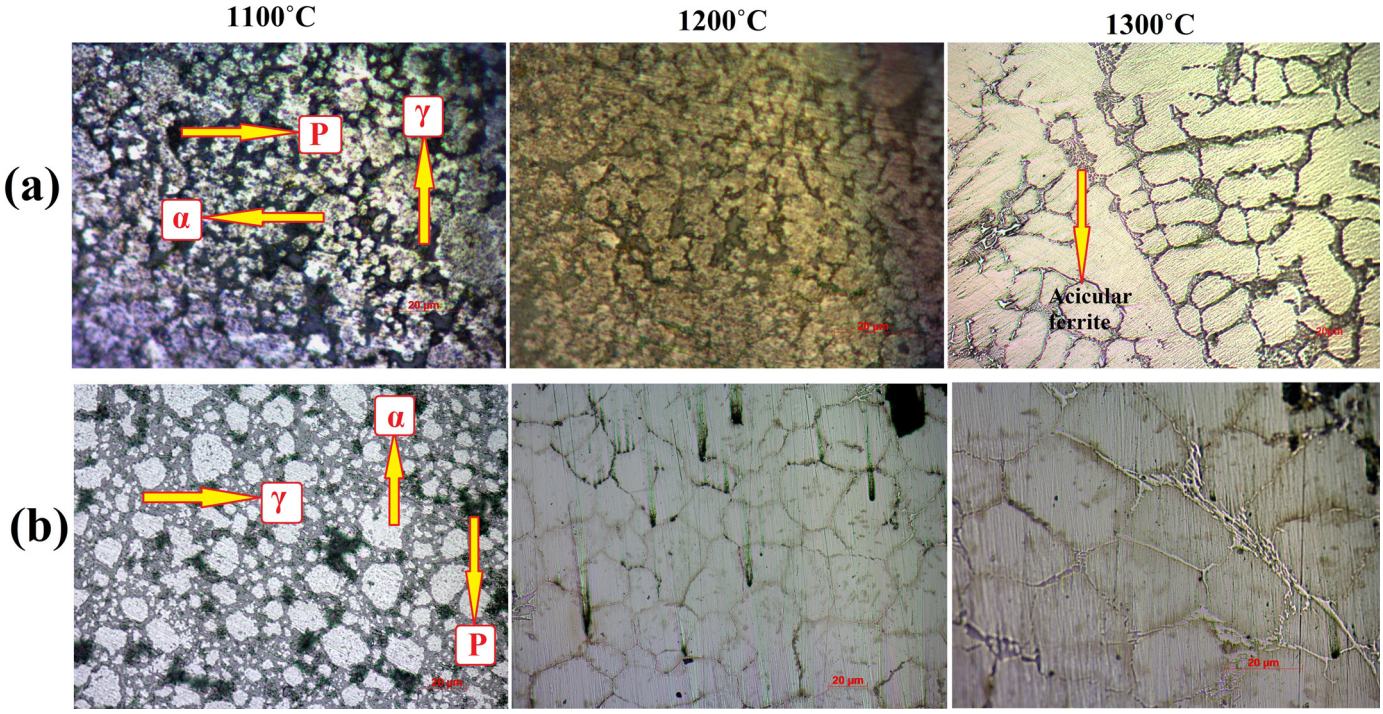

Fig. 7. Optical microstructure of (a) duplex and (b) ferritic stainless steel samples sintered at 1100, 1200 and 1300°C in argon atmosphere (α-Ferrite, γ-Austenite and P-Pores)

samples are represented in figure 8(a). The density of both the stainless steel samples increases with the increase in sintering temperature from 1100 to 1300°C. This is due to low porosity and higher amount of shrinkage at higher sintering temperature. As temperature increases the rate of mass transfer increases and eventually results in formation of neck and better bonding between powder particles. At 1300°C, the rate of diffusion is more effective due to the efficient transfer of mass through necking mechanism. Hence, a maximum density of 90% is achieved for both duplex and ferritic stainless steel samples at 1300°C sintering temperature. Optical microstructure of duplex and ferritic stainless steel samples confirms that the increase in sintering temperature decreases the number of pores and increases the density. The density of duplex and ferritic stainless steels varies from 77% to 90% and from 78% to 91% respectively at sintering temperature of 1100 to 1300°C.

Figure 8(b) represents the Vickers microhardness values of duplex and ferritic stainless steel samples measured at 245 mN indentation load. As we discussed, at higher sintering temperature, density increases due to the reduced porosity ratios and hence hardness increases. Duplex stainless steel samples show more hardness values than ferritic stainless steels. The Vickers microhardness values of duplex and ferritic stainless steels vary from 270 to 497 HV and 199 to 252 HV respectively, for variation of sintering temperature from 1100 to 1300°C.

The effect of indentation load on the microhardness of duplex and ferritic stainless steel samples sintered at 1100, 1200 and 1300°C respectively are shown in figure 9(a) and 9(b) respectively. The Vickers microhardness measurements were carried out at three different indentation loads of 98, 245 and 490 mN with a dwell time of 10 seconds for both the stainless steel samples. For each stainless steel sample, at least five trials of the indentations were made at each load and the average values of the diagonal lengths of the indentation marks were measured as hardness [22].

From figure 9, it is confirmed that the microhardness values of both the stainless steel sample decrease with the increase in applied indentation load. This is due to the indentation size effect (ISE), and it occurs due to the surface effect and strain gradient effect [21,43]. ISE also directly relates to the intrinsic structural

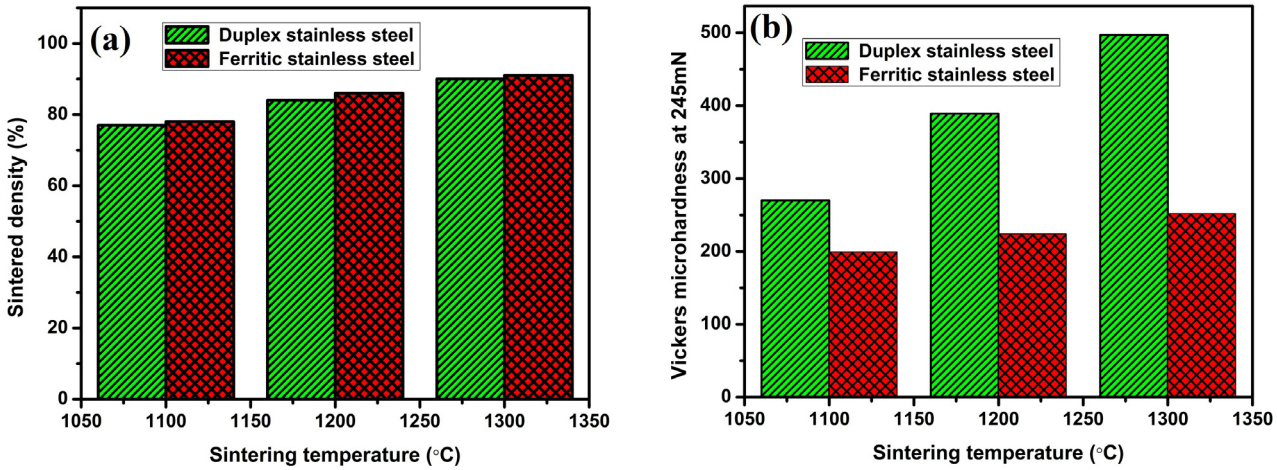

Fig. 8. Graphs of (a) sintered density and (b) Vickers microhardness at 245 mN of both duplex and ferritic stainless steel stainless steel samples sintered at 1100, 1200 and 1300°C in argon atmosphere

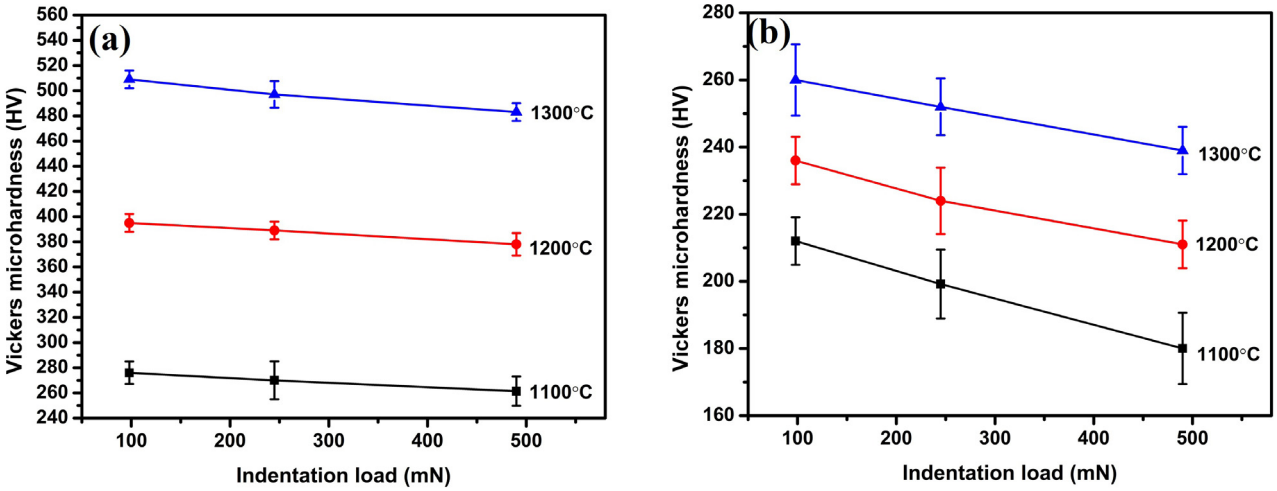

Fig. 9. Effect of indentation load (98, 245 and 490 mN) on Vickers microhardness of (a) duplex and (b) ferritic stainless steel samples sintered at 1100, 1200 and 1300°C in argon atmosphere

factors of the tested materials such as indentation elastic recovery, work hardening during indentation and surface dislocation pining [44,45]. From the figure we can conclude that indentation load and microhardness are inversely proportional to each other. Mott [46], Buckle [47] reported the substantial variations of hardness with depth, especially at depths of less than a few micrometers. They concluded that there are possibility of two types of effects; normal ISE and reverse ISE. Generally, normal ISE increases the hardness at smaller depths, and reverse ISE decreases the hardness. But in our case, the microhardness decreases with the increase in the indentation depth due to normal ISE.

4. Conclusions

In the present study, we have successfully prepared nano-structured duplex and ferritic stainless steel powders from elemental Fe, Cr and Ni powders by both dry and wet planetary milling and compared. Dry milling results in spherical shape of stainless steel powders; whereas in wet milling one can observe irregular shape of particles. Milling of stainless steel samples carried out at argon atmosphere shows reduced particle size as well as lower crystallite size and higher lattice strain as compared to milling carried out at toluene atmosphere. XRD spectrum of dry milled duplex stainless steel exhibit rapid phase transformation from α-Fe to γ-Fe than wet milled duplex stainless steel; this is due to the high impact energy, increased defects and frequent collision of ball-powder-jar. An increase in sintering temperature from 1100 to 1300°C increases the density and hardness of the samples and decreases the porosity ratios. Due to ISE, both the stainless steel samples show reduced hardness with an increasing indentation load. Both duplex and ferritic stainless steels show maximum density and hardness at 1300°C. Density and microhardness values of 90% and 497 HV were obtained for duplex stainless steel. Similarly, ferritic stainless steel exhibits 91% sintered density and 252 HV microhardness value. Finally, we can conclude that milling atmosphere plays a very important role in refining the powder size, morphology and phase transition.

REFERENCES

[1] L.A. Dobrzanski, Z. Brytan, M. Actis Grande, M. Rosso, Arch. Mater. Sci. Eng. **28**, 217-223 (2007).

[2] S. Herenu, I. Alvarez-Armas, A.F. Armas, Scripta Mater. **45**, 739-745 (2001).

[3] H. Miyamoto, T. Mirnaki, S. Hashimoto, Mater. Sci. Eng. A. **319**, 779-783 (2001).

[4] M.J. Schofield, R. Bradsha, R.A. Cottis, Mater. Perform. **35**, 65-70 (2009).

[5] R. Shashanka, D. Chaira, Powder Technology. **278**, 35-45 (2015).

[6] K.J. Kurzydłowski, Bull. Pol. Acad. Sci. Tech. Sci. **52**, 275 (2004).

[7] Austral Wright Metals, Stainless Steel-Properties and Applications of Ferritic Grade Stainless Steel, Aug 31, 2008.

[8] R. Shashanka, B.E. Kumara Swamy, S. Reddy, D. Chaira, Anal. Bioanal. Electrochem. **5**, 455-466 (2013).

[9] Sathish Reddy, B.E. Kumara Swamy, S. Arun, Mohan Kumar, R. Shashanka, H. Jayadevappa, Chemical Sensors. **2**, 1-8 (2012).

[10] C. Suryanarayana, Prog. Mater. Sci. **46**, 1-184 (2001).

[11] A.K. Nayak, R. Shashanka, D. Chaira, 5th National Conference on Processing and Characterization of Materials, IOP Conf. Series: Materials Science and Engineering, **115**, 012008 (2016).

[12] R. Shashanka, Anal. Bioanal. Electrochem. **10**, 349-361 (2018).

[13] R. Shashanka, International Journal of Scientific & Engineering Research. **8**, 588-594 (2017).

[14] Hye Jin Jung, Youngku Sohn, Hong Gye Sung, Hyung Soo Hyun, Weon Gyu Shin, Powder Technology. **269**, 548-553 (2015).

[15] Union Process, Planetary Ball Mills 101, Union Process, Inc. 1925 Akron-Peninsula Road, Akron, Ohio, Aug 21, 2017. https://www.unionprocess.com/planetary-ball-mill-basics.html

[16] R. Shashanka, D. Chaira, Powder Technol. **259**, 125-136 (2014).

[17] I. Ismail, M. Hashim, K.A. Matori, R. Alias, J. Hassan, J. Magn. Magn. Mater. **323**, 1470-1476 (2011).

[18] R. Shashanka, D. Chaira, B.E. Kumara Swamy, Int. J. Electrochem. Sci. **10**, 5586-5598 (2015).

[19] R. Shashanka, D. Chaira, B.E. Kumara Swamy, International Journal of Scientific & Engineering Research. **6**, 1863-1871 (2015).

[20] R. Shashanka, D. Chaira, B.E. Kumara Swamy, International Journal of Scientific & Engineering Research. **7**, 1275-1285 (2016).

[21] R. Shashanka, D. Chaira, Mater Charact. **99**, 220-229 (2015).

[22] R. Shashanka, D. Chaira, D. Chakravarty, Journal of Materials Science and Engineering B. **6** (5-6), 111-125 (2016).

[23] R. Shashanka, D. Chaira, Acta Metall. Sin. (Engl. Lett.) **29**, 58-71 (2016).

[24] R. Shashanka, D. Chaira, Tribology Transactions. **60**, 324-336 (2017).

[25] S. Pandya, K.S. Ramakrishna, A.R. Annamalai, A. Upadhyaya, Mater. Sci. Eng. A. **556**, 271-277 (2012).

[26] K. Vijayalakshmi, V. Muthupandi, R. Jayachitra, Mater. Sci. Eng. A. **529**, 447-451 (2011).

[27] P. Guiraldenq, O.H. Duparc, Metall. Res. Technol. **114**, 613 (2017).

[28] D.A. Huerta, Victor Sosa, M.C. Vargas, J.C. Ruiz-Suarez, Phys. Rev. E. **72**, 031307 (2005).

[29] Lauren Juliet Ayers, The hardening of type 316 L stainless steel welds with thermal aging, Massachusetts Institute of Technology, 2012.

[30] B.D. Cullity, S.R. Stock, Elements of X-Ray diffraction, Pearson, 2003. (Paperback, ISBN-13: 9780131788183).

[31] S. Gupta, R. Shashanka, D. Chaira, 4th National Conference on Processing and Characterization of Materials, IOP Conf. Series: Materials Science and Engineering. **75**, 012033 (2015).

[32] Q. Meng, N. Zhou, Y. Rong, S. Chen, T.Y. Hsu, Xu Zuyao, Acta. Mater. **50**, 4563-4570 (2002).

[33] M.H. Enayati, M.R. Bafandeh, J. Alloy. Compd. **454**, 228-232 (2008).

[34] T. Haghir, M.H. Abbasi, M.A. Golozar, M. Panjepour, Mater. Sci. Eng. A. **507**, 144-148 (2009).

[35] M. Wang, H. Sun, L. Zou, G. Zhang, S. Li, Z. Zhou, Powder. Technol. **272**, 309-315 (2015).

[36] F. Tehrani, M.H. Abbasi, M.A. Golozar, M. Panjepour, Mater. Sci. Eng. A.**528**, 3961-3966 (2011).

[37] E. Salahinejad, M.J. Hadianfard, M. Ghaffari, R. Amini, Sh. Bagheri Mashhadi, A.K. Okyay, Adv. Powder. Tech. **24**, 605-608 (2013).

[38] S. Noh, B.K.. Choi, S.H. Kang, T.K. Kim, Nucl. Eng. Technol. **46**, 857-862 (2014).

[39] M. Gojic, A. Nagode, B. Kosec, S. Kozuh, S. Savli, T. Holjevac Grguric, L. Kosec, Eng. Fail. Anal. **18**, 2330-2335 (2011).

[40] R. Shashanka, D. Chaira, B.E. Kumara Swamy, Archives of Metallurgy and Materials. **63**, 749-763 (2018).

[41] Bhadeshia, H.K.D. Hansraj, Honeycombe, R.W. Kerr, Steels: Microstructure and Properties (3rd ed.), Butterworth-Heinemann, (2006). ISBN 978-0-7506-8084-4.

[42] R.A. Ricks, G.S. Barritte, P.R. Howell, Proc. Int. Conf. on Solid-Solid Phase Transformations, Natural Science Foundation/Met. Soc. AIME 463-8 (1982).

[43] I. Manika, J. Maniks, Acta Mater. **54**, 2049-2056 (2006).

[44] J.H. Gong, J.J. Wu, Z.D. Guan, J. Eur. Ceram. Soc. **19**, 2625-2631 (1999).

[45] H. Buckle, in: The Science of Hardness Testing and Its Research Application, ed. by J.H. Westbrook, H. Conrad, ASM, Metal Park, 453 (1973).

[46] B.W. Mott, Micro-indentation Hardness Testing, Butterworths Scientific Publications, London, 1956.

[47] H. Buckle, Metall. Rev. **4**, 49-100 (1959).